PHOTONIC SENSORS / Vol. 11, No. 3, 2021: 341–349

Mach-Zehnder Interferometer for High Temperature (1 000 ℃) Sensing Based on a Few-Mode Fiber

Juan LIU, Chaowei LUO, Hua YANG, Zhen YI, Bin LIU*, Xingdao HE, and Qiang WU

Key Laboratory of Nondestructive Testing, Ministry of Education, Nanchang Hangkong University, Nanchang 330063, China

*Corresponding author: Bin LIU E-mail: liubin_d@126.com

Abstract: A Mach-Zehnder interferometer (MZI) for high temperature (1 000℃) sensing based on few mode fiber (FMF) was proposed and experimentally demonstrated. The sensor was fabricated by fusing a section of FMF between two single-mode fibers (SMFs). The structure was proven to be an excellent high temperature sensor with good stability, repeatability, and high temperature sensitivity (48.2 pm/℃) after annealing process at a high temperature lasting some hours, and a wide working temperature range (from room temperature to 1 000℃). In addition, the simple fabrication process and the low cost offered a great potential for sensing in high temperature environments.

Keywords: Mach-Zehnder interferometer; annealing process; few mode fiber; high temperature sensing

Citation: Juan LIU, Chaowei LUO, Hua YANG, Zhen YI, Bin LIU, Xing Dao HE, *et al*., "Mach-Zehnder Interferometer for High Temperature (1 000 ℃) Sensing Based on a Few-Mode Fiber," *Photonic Sensors*, 2021, 11(3): 341–349.

1. Introduction

Optical fiber sensors have attracted growing interest for many industrial applications because of their attractive features, such as miniaturization, immunity to electromagnetic radiation, high stability and reliability, extraordinary resistance to corrosive environments, and the possibility of remote interrogation from long distances [1–3]. The applications of some sensors require the ability to work at very high temperatures with good stability and accuracy. Temperature sensors based on optical fiber can be mainly categorized into two types depending on the physical principle of sensor operation. The first type includes grating based temperature sensors while the second type includes sensors whose operation is based on interferometry. A fiber Bragg grating (FBG) temperature sensor reflects one particular wavelength and the reflected wavelength can vary with the ambient temperature. Moreover, several of these sensors can be multiplexed in a series along with a single optical fiber so that a single instrument can simultaneously monitor many individual sensors. However, the FBG sensor exhibits poor stability in a high-temperature environment and the grating can be completely erased at temperatures around 700 ℃ [4]. FBG-based temperature sensors are usually used at temperatures under 200 ℃ due to the decay of the FBG's reflectivity [5]. Naturally, some types of FBG sensors can work stably at 1 000 ℃ by utilizing an intensive ultraviolet (UV) laser source or a femtosecond pulse duration infrared (fs-IR) laser source to inscribe gratings. However, the fabrication

Received: 24 November 2019 / Revised: 01 June 2020
© The Author(s) 2020. This article is published with open access at Springerlink.com
DOI: 10.1007/s13320-020-0596-z
Article type: Regular

process for such gratings is rather complicated and expensive [6]. A large variety of fiber optic temperature sensors based on single-mode fiber (SMF) configurations and special fibers have been proposed for operation at high temperatures. These sensors use multimode fibers, thin core fibers, micro cavities, micro channels, twin cores, multi-core fibers, hollow core fiber, and photonic crystal fibers (PCF) [7–16]. The single-mode fiber (SMS) structure has low sensitivity because the interference is confined in the same core of the multimode fiber, which has identical thermal properties [15]. Micro cavities fabricated on capillary fiber tips, microchannel-drilled fiber cores, and micro structured fiber tapers require complicated fabrication processes, such as laser micromachining or chemical etching which is difficult to reproduce and needs expensive equipment. In recent years, new sensors based on few-mode optical fibers have attracted the interest of researchers. Compared with single-mode optical fiber sensors, few-mode optical fiber sensors have unique advantages such as simple structure, strong anti-noise ability, high sensitivity, and mode controllability. Paralleled Mach-Zehnder interferometer (MZI) in few-mode multicore fiber (FM-MCF) for temperature and strain discriminative sensing was proposed and experimentally demonstrated by Zhan *et al*. [17]. Due to the low condition number of the cross coefficient matrix dependent on the temperature and strain response indexes, the temperature-strain cross sensitivity can be efficiently eliminated. The relationship between the temperature/strain wavelength sensitivity of MZI and the wavelength separation of the measured wavelength to the critical wavelength was studied by Lu *et al*. [18]. The in-line MZI fiber optic sensor has been constructed by splicing a section of specially designed few-mode fiber (FMF).

In this paper, a novel high temperature sensor for MZI based on the FMF is proposed, for which a section of the FMF was fusion spliced between two SMFs. The transmission fiber was spliced to the FMF by offsetting several micrometers at the input, and the other side of the FMF was spliced to another SMF by keeping the core aligned at the output. The proposed structure demonstrated a high temperature sensitivity of about 48.2 pm/℃ and a wide working temperature range (from 100 ℃ to 1 000 ℃). The structure was proven to be an excellent high temperature sensor with good stability and repeatability after annealing at a high temperature. In addition, the simple fabrication process and the low cost offer a great potential for application.

2. Fabrication and operation principle

The FMF used in the experiment was four-mode optical fibers (step-type) provided by YOFC (Yangtze optical fiber and cable). It supported four modes, namely, LP_{01}, LP_{11}, LP_{21}, and LP_{02}. A schematic diagram of the proposed SMF-FMF-SMF fiber structure is shown in Fig. 1.

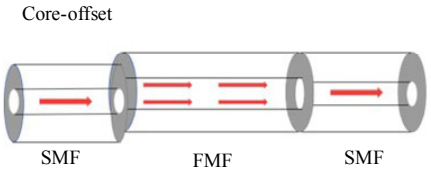

Fig. 1 Schematic diagram of the proposed SMF-FMF-SMF fiber structure.

The input light was injected from the lead-in SMF to the FMF and the high-order modes could be excited at the first splicing point. The fundamental mode and the high-order modes propagated in the FMF simultaneously. In order to control the excited energy of the higher-order mode and basic mode and achieve a good interference extinction ratio, a core-offset splicing was adopted at the first splicing point. At the second splicing point, the high-order modes were coupled back into the lead-out core of the SMF and interfered with the fundamental mode. In order to decrease the loss and avoid the cladding mode entering the fiber core at the second splicing point, the output section of the FMF was not core-offset spliced with the single-mode fibers.

To further examine the working principle, we analyzed the sensor's responses to temperature. The

intensity at the output of the sensor can be described as

$$I(\lambda) = I_1 + I_2 + 2\sqrt{I_1 I_2}\cos\varphi \tag{1}$$

where I_1 and I_2 are the optical powers of the two modes involved, and λ is the wavelength of the incident light. φ represents the phase difference between the two modes after transmission in the fiber, and it can be described as

$$\varphi = \frac{(2\pi\Delta n_{\text{eff}} L)}{\lambda} \tag{2}$$

where Δn_{eff} represents the effective refractive index difference between modes involved in the interference and L is the length of the FMF. When $\varphi=(2m+1)\pi$ ($m=0, \pm1, \pm2, \cdots$), the intensity takes the minimum value. Therefore, the resonant wavelength dip λ_{mdip} can be expressed as

$$\lambda_{\text{mdip}} = \frac{2\Delta n_{\text{eff}} L}{(2m+1)}. \tag{3}$$

When the ambient temperature of the MZIs structure varies, the resonant wavelength will shift due to the changes of the effective refractive index of transmission modes and the fiber length. The wavelength shift can be expressed as [19]

$$\begin{aligned}\Delta\lambda_{\text{mdip},T} &= \lambda_{\text{mdip},T+\Delta T} - \lambda_{\text{mdip},T} \\ &= \frac{2(\Delta n_{\text{eff}} + \Delta n_T)(L+\Delta L)}{(2m+1)} - \frac{2\Delta n_{\text{eff}} L}{(2m+1)}\end{aligned} \tag{4}$$

where Δn_T and ΔL are the effective refractive index and the fiber length difference changed with ΔT, respectively. Δn_T is mainly determined by the thermal-optic coefficient while ΔL is related to the thermal-expansion coefficient. Since $\Delta L/L$ is apparently small, the thermal expansion can be neglected. Hence, the wavelength shift can be simplified as [20]

$$\Delta\lambda_{\text{mdip},T} = \frac{\Delta n_T}{\Delta n_{\text{eff}}}\lambda_{\text{mdip}}. \tag{5}$$

According to (5), the temperature sensitivity is determined by Δn_T and Δn_{eff}, and different excited high-order modes show distinct temperature sensitivities.

In order to investigate the propagating modes contributing to the interferences, we performed the following work. The mode field distributions of the transmission modes in the FMF were calculated by using the finite element method (COMSOL Multiphysics), as shown in Fig. 2.

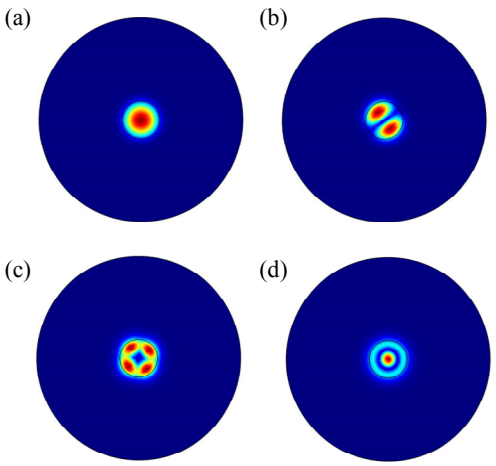

Fig. 2 Mode field distribution of the transmission mode: (a) LP_{01}, (b) LP_{11}, (c) LP_{21}, and (d) LP_{02} in the FMF.

According to mode field distributions, the effective refractive index differences between the LP_{01} mode and the other high modes were calculated. The effective refractive indices of four modes were 1.467 0, 1.466 0, 1.464 7, and 1.464 2, so the refractive index differences between the LP_{01} mode and the other high modes were 0.001 0, 0.002 3, and 0.002 8, respectively. Then the interference spectra of mode LP_{01} with modes LP_{11}, LP_{21}, and LP_{02} for an FMF length of 3 cm were calculated, as shown in Figs. 3(a), 3(b), and 3(c), and the corresponding free spectral ranges (FSRs) were 86 nm, 37 nm, and 29 nm, respectively. In the experiment, we fabricated an FMF structure with a length of 3 cm and tested its interference spectrum by using an sc-5-fc super continuous spectrum source with an output wavelength range from 1 200 nm to 1 650 nm and an optical spectrum analyzer (OSA, AQ6370) with a resolution of 0.02 nm as shown in Fig. 3(d). By comparison and analysis, it was found that the experimental interference spectrum was agreed with the theoretical interference spectrum between mode

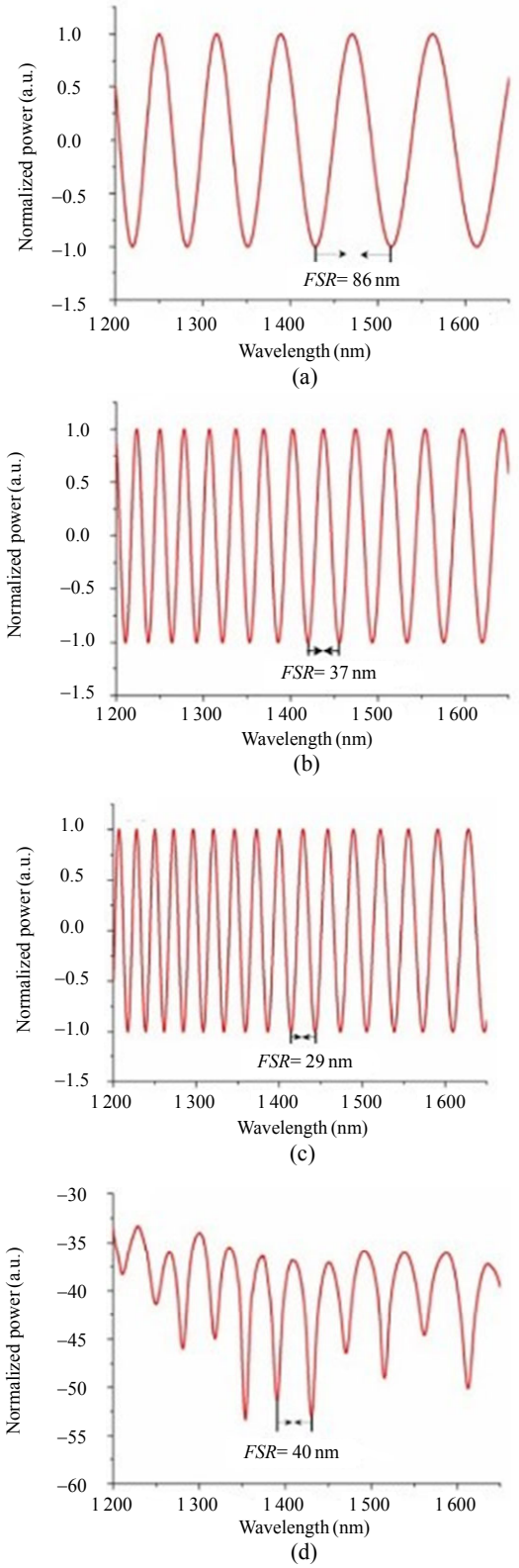

Fig. 3 Simulated interference spectrum and measured transmission spectrum: (a) simulated interference spectrum between mode LP_{01} and mode LP_{11}, (b) simulated interference spectrum between mode LP_{01} and mode LP_{21}, (c) simulated interference spectrum between mode LP_{01} and mode LP_{02}, and (d) measured transmission spectrum.

LP_{01} and mode LP_{21}. Therefore, the interference spectrum of the FMF structure was mainly caused by mode interference between LP_{01} and LP_{21}.

When only the core mode LP_{01} and the higher mode LP_{21} are taken into consideration, the extinction ration (ER) of the interferometer can be written as [21]

$$ER = 10\lg\left[\left(1+\sqrt{I_2/I_1}\right)\Big/\left(1-\sqrt{I_2/I_1}\right)\right]^2 \qquad (6)$$

where I_1 and I_2 are the intensities of the core mode LP_{01} and the higher mode LP_{21}. According to (6), in order to obtain a higher extinction ratio in the transmission spectrum of the interferometer, the ratio of I_1/I_2 should be close to 1. Due to the design of core-offset, we can achieve a good interference extinction ratio by adjusting the displacement offset. The relationship between the ER and the displacement offset was investigated in the experiment. The transmission spectra of the sensor proposed are shown in Fig. 4. It could be seen that the *ER* of the spectra increased with the core-offset increases, but the loss increased as well. The *ER*s were 3.32 dB, 11.83 dB, 13.80 dB, 18.77 dB, and 20.94 dB, respectively, corresponding with the core-offset of 5 μm, 7.5 μm, 10 μm, 12.5 μm, and 15 μm. When the core-offset was 5 μm, it was difficult to distinguish the dip of the spectral envelope. When the core-offset reached 15 μm, the loss was too high to observe the spectra. We set the core-offset to be 12.5 μm for comprehensive consideration.

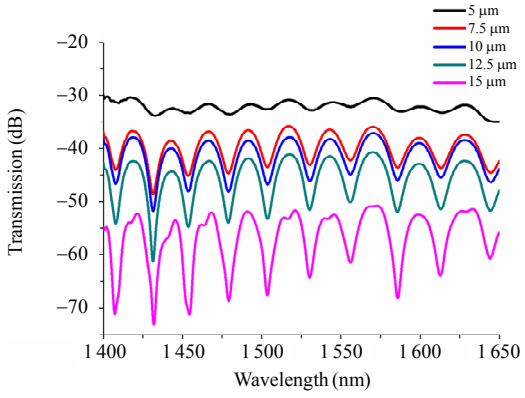

Fig. 4 Transmission spectra with different core-offsets.

The *FSR* can be expressed as [20]

$$FSR = \frac{\lambda^2}{\Delta n_{\text{eff}} L}. \tag{7}$$

As large *FSR* avoids the overlapping reading problem and can provide wider working range, it is very important to choose the appropriate FMF length.

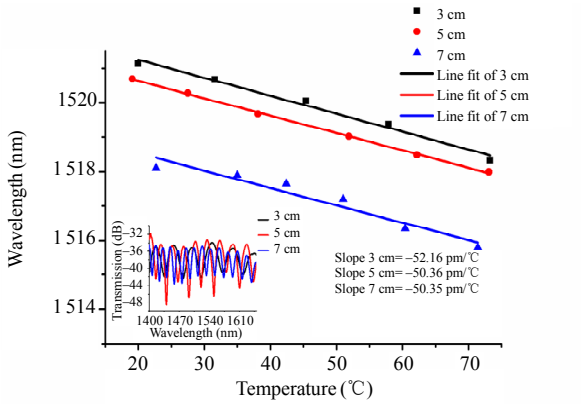

Fig. 5 Transmission spectrum based on the structure with different lengths of the FMF and measured temperature sensitivity.

Figure 5 shows the experimentally measured transmission spectrum based on the structure with different lengths of the FMF. It can be seen that the spectral periodicity of the transmission signal increased with the lengths of the FMF in the spectral domain, which also means that the FSR decreased accordingly. The temperature sensitivity of the structure with these three lengths of FMF was measured below 80 ℃. It should be noted that the temperature sensitivity had little change with the length as shown in Fig. 5. The following study in the paper was carried out with an FMF length of 3 cm.

3. Experimental results and discussion

Experimental investigations into the temperature and strain sensing based on the above structure were carried out. Figure 6 shows the experimental setup for the measurement of temperature and strain.

In order to avoid any impact induced by bending, the input and the output SMF ends were fixed to two manual translation stages and the ends were straightened. The straight FMF section was placed inside the furnace. The furnace used in the measurement was with a length of heating zone about 20 cm and could provide a temperature range from room temperature up to 1 200 ℃. The transmitted light from the SMF output port was monitored by an optical spectrum analyzer (OSA) of AQ6370.

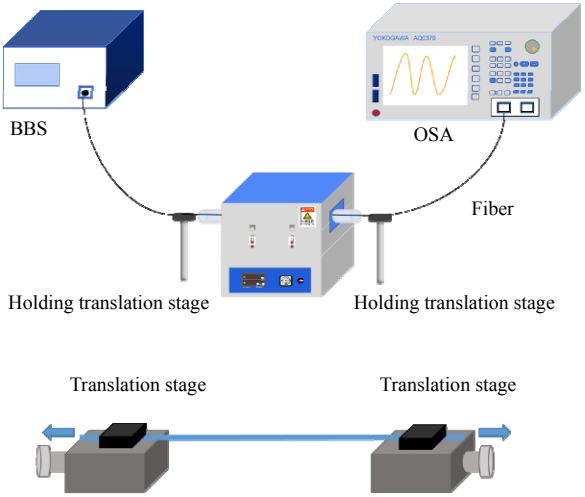

Fig. 6 Schematic diagram of the experimental configuration test platform for stress sensing.

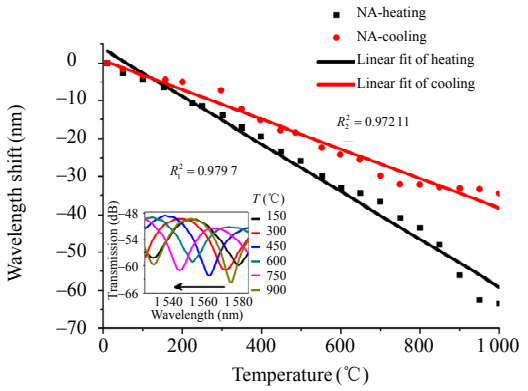

Fig. 7 Wavelength shift versus temperature for the FMF sensor.

The temperature sensing performance was studied with an approximately 3-cm long FMF. The spectra were recorded stepwise by heating and cooling down the furnace. As shown in Fig. 7, the sensor demonstrated a linearity between the wavelength shift and the temperature variation, but the actually measured points existed some slight fluctuation when the temperature rose to 600 ℃. Besides, the temperature sensitivities of the sensor

were a little different in the heating and cooling process. The wavelength shifts of the sensor in the two processes were mismatched, indicating that the sensor's stability deteriorated with the temperature.

Except for the measurements error, one of the important factors causing the above phenomena was the residual stress and thermal memory that existed in the fiber structure [7, 22]. In referring to [16] and the melting point of the optical fiber (between 1 600 ℃ and 1 700 ℃), an annealing process was introduced with the goal of eliminating all of the residual stress in the FMF structure. The structure was first subjected to an annealing process, being heated up to 950 ℃ and maintained at this temperature for about 0.5 h. It was then passively cooled down until it reached room temperature. After the 0.5-hour annealing process, the transmission spectra of the sensor at different temperatures were recorded by heating up and cooling down the furnace. Figure 8 shows the wavelength versus temperature variations after the 0.5-hour annealing process. It can be seen that the sensor's stability was optimized after the annealing process. But the annealing process for 0.5 h was not enough to eliminate the residual stress in the FMF.

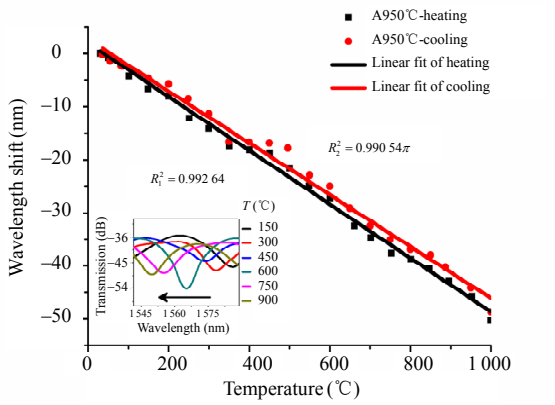

Fig. 8 Wavelength shift versus temperature for the sensor after the 0.5-hour annealing process.

In order to eliminate the effect of the residual stress in the FMF structure completely, we took another FMF sensor with the same length to do the annealing process for 2 h.

The evolution of the wavelength shift during the process was recorded as shown in Fig. 9(a). During the annealing process, a blue shift was observed in the first 50 minutes and then the sensor transmission spectrum stabilized and remained stable throughout the last 70 minutes.

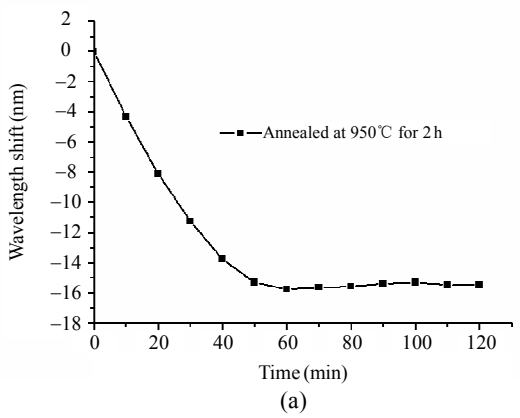

(a)

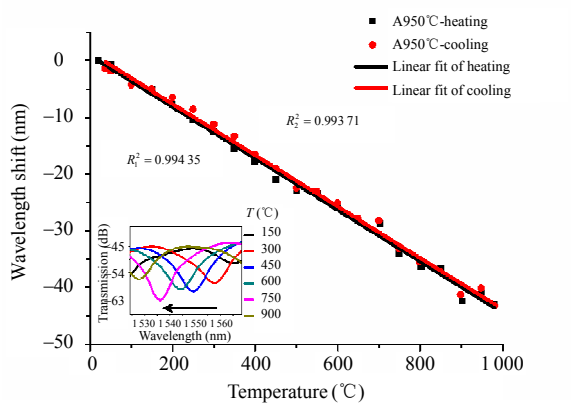

(b)

Fig. 9 Process of annealing at 950℃ for 2 h: (a) time evolution of the wavelength shift and (b) wavelength shift versus temperature for the FMF sensor after the annealing process.

The high-temperature sensing characteristics from room temperature to 1 000 ℃ were then studied. The wavelength shift versus temperature for heating cycle and cooling cycle is shown in Fig. 9(b). The curves were linearly fitted with the *R*-square values of both above 0.99 and a temperature sensitivity of 48.2 pm/℃ was achieved. The measured wavelength shift matched well in the heating and cooling cycles, which clearly demonstrates that the stability of the sensor had a significant improvement after an annealing process for 2 h.

The repeatability and reliability of the sensor

after an annealing process were also tested, as shown in Fig. 10. Three measurements about temperature sensing (from room temperature to 1000℃) were carried out with the same sensor. And after two days, a repetitive experiment was also performed. The results showed good repeatability and reliability.

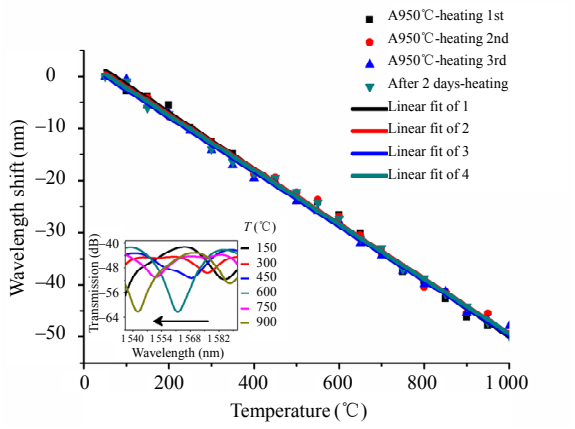

Fig. 10 Test of repeatability and reliability about wavelength shift versus temperature for the sensor after the annealing process.

Further study about the effect of annealing temperature on the sensor performance was done. Other FMF temperature sensors with lengths of 3 cm were exposed to 1 000 ℃ for 2 h, and the evolution of the wavelength shift during the process was recorded, as shown in Fig. 11(a). During the annealing process, a blue shift was observed in the first 30 minutes and then the sensor transmission spectrum stabilized and remained stable throughout the last 90 minutes. Figure 11(b) shows the wavelength versus temperature variations after the 2-hour annealing process. It can be seen that after a 2-hour annealing process at 1 000 ℃, the wavelength shift in the heating process was consistent with it in the cooling process. It demonstrated the same temperature sensitivity of about 47.9 pm/℃.

A very stable response from the sensor was achieved after several hours of the annealing process under high-temperature conditions. As shown in Figs. 9(a) and 11(a), the wavelength shift changed little after 55 min and 40 min, respectively. The higher temperature improved the annealing efficiency. The small difference of temperature sensitivity indicated the temperature of annealing process had little effect on the temperature sensitivity. And the errors arose from the structural fabrication process.

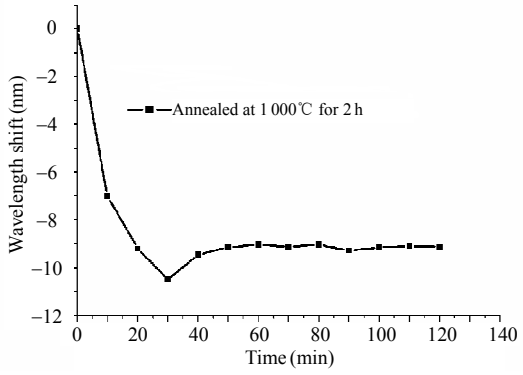

(a)

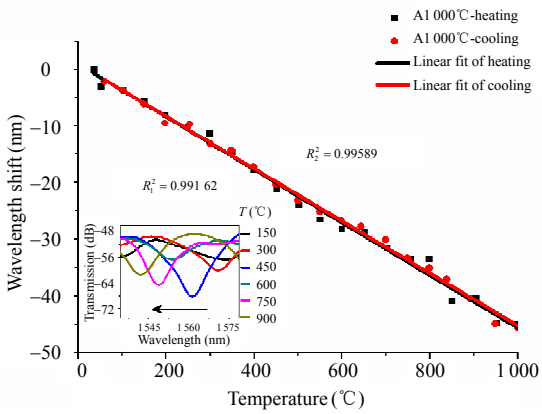

(b)

Fig. 11 Process of annealing at 1000 ℃ for 2 h: (a) time evolution of the wavelength shift and (b) wavelength shift versus temperature for the sensor after the annealing process.

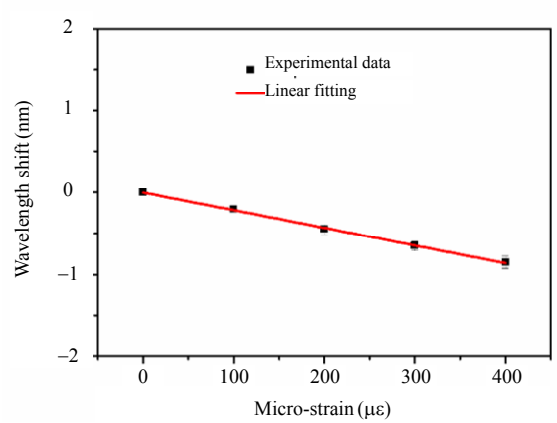

Fig. 12 Wavelength shift versus micro-strain.

The strain sensing performance of the MZI sensors was tested before the annealing. Figure 12

shows the strain response curve and the sensitivity reached –1.5 pm/με. Compared with the temperature response, the MZI sensor was insensitive to the strain change. The structure was easily broken under micro stress after the annealing process.

4. Conclusions

In this work, we proposed and investigated a very simple device for high-temperature sensing based on few-mode fibers. After the 2-hour annealing process, the sensor showed high stability and repeatability for the temperature measurement from room temperature to 1 000 ℃, with a sensitivity of about 48.2 pm/℃. The strain sensitivity of the sensor was –1.5 pm/με. Therefore, the temperature-strain cross-sensitivity of the sensor was only 0.031 1 ℃/με, and it could be a strain insensitive and high temperature fiber sensor. Through theoretical and experimental analysis, due to the wide FSR and the suitable extinction ratio of the interference pattern, this fiber Mach-Zehnder interferometer based on the FMF could guarantee an accurate temperature measurement in a large range. The simple structure, cost-effective fabrication process, high sensitivity, excellent stability and repeatability, and wide measurement range make this compact device a good candidate for practical application in the future.

Acknowledgment

This work was funded by the National Natural Science Foundation of China (NSFC) (Grant Nos. 41266001, 61665007, and 61865013); National Key Research and Development Project from the Ministry of Science and Technology (Grant No. 2018YFE0115700); Science and Technology Project of Jiangxi Education Department (Grant No. GJJ180518); Nanchang Hangkong University graduate student innovation special fund project (Grant No. YC2019053).

Open Access This article is distributed under the terms of the Creative Commons Attribution 4.0 International License (http://creativecommons.org/licenses/by/4.0/), which permits unrestricted use, distribution, and reproduction in any medium, provided you give appropriate credit to the original author(s) and the source, provide a link to the Creative Commons license, and indicate if changes were made.

References

[1] F. T. S. Yu, P. B. Ruffin, and S. Yin, "*Fiber optic sensors*," New York: CRC Press, 2008.

[2] D. Liu, A. K. Mallik, J. Yuan, C. Yu, G. Farrell, Y. Semenova, *et al*., "High sensitivity refractive index sensor based on a tapered small core single-mode fiber structure," *Optics Letters*, 2015, 40(17): 4166–4169.

[3] W. Yu, T. Lang, J. Bian, and W. Kong, "Label-free fiber optic biosensor based on thin-core modal interferometer," *Sensors and Actuators B: Chemical*, 2016, 228(2): 322–329.

[4] G. Brambilla, "High-temperature fibre Bragg grating thermometer," *Electronics Letters*, 2002, 38(17): 954–956.

[5] S. R. Baker, H. N. Rourke, V. Baker, and D. Goodchild, "Thermal decay of fiber Bragg gratings written in boron and germanium codoped silica fiber," *Journal of Lightwave Technology*, 1997, 15(8): 1470–1477.

[6] S. Li-Yang, T. Wang, J. Canning, K. Cook, and T. Hwa-Yaw, "Bulk regeneration of optical fiber Bragg gratings," *Applied Optics*, 2012, 51(30): 7165–7169.

[7] J. E. Antonio-Lopez, Z. S. Eznaveh, P. LiKamWa, A. Schülzgen, and R. Amezcua-Correa, "Multicore fiber sensor for high-temperature applications up to 1000 ℃," *Optics Letters*, 2014, 39(15): 4309–4312.

[8] J. Zhu, A. Zhang, T. H. Xia, S. He, and W. Xue, "Fiber-optic high-temperature sensor based on thin-core fiber modal interferometer," *IEEE Sensors Journal*, 2010, 10(9): 1415–1418.

[9] Y. Liu, S. Qu, and Y. Li, "Single microchannel high-temperature fiber sensor by femtosecond laser-induced water breakdown," *Optics Letters*, 2013, 38(3): 335–337.

[10] Y. Zhang, L. Yuan, X. Lan, A. Kaur, J. Huang, and H. Xiao, "High-temperature fiber-optic Fabry-Perot interferometric pressure sensor fabricated by femtosecond laser," *Optics Letters*, 2013, 38(22): 4609–4612.

[11] P. Rugeland and W. Margulis, "Revisiting twin-core fiber sensors for high-temperature measurements," *Applied Optics*, 2012, 51(25): 6227–6232.

[12] G. Coviello, V. Finazzi, J. Villatoro, and V. Pruneri, "Thermally stabilized PCF-based sensor for temperature measurements up to 1000 ℃," *Optics*

Express, 2009, 17(24): 21551–21559.

[13] C. Wu, H. Y. Fu, K. K. Qureshi, B. O. Guan, and H. Y. Tam, "High-pressure and high-temperature characteristics of a Fabry-Perot interferometer based on photonic crystal fiber," *Optics Letters*, 2011, 36(3): 412–414.

[14] M. Janik, M. Koba, P. Mikulic, W. J. Bock, and M. Śmietana, "Combined long-period grating and micro-cavity in-line Mach-Zehnder interferometer for refractive index sensing," in *2017 25th Optical Fiber Sensors Conference (OFS)*, Korea, April 24–28, 2017, pp. 1–4.

[15] Y. Liu and L. Wei, "Low-cost high-sensitivity strain and temperature sensing using graded-index multimode fibers," *Applied Optics*, 2007, 46(13): 2516–2519.

[16] D. Liu, Q. Wu, C. Mei, J. Yuan, X. Xin, A. K. Mallik, *et al*., "Hollow core fiber based interferometer for high-temperature (1 000°C) measurement," *Journal of Lightwave Technology*, 2017, 36(9): 1583–1590.

[17] X. Zhan, Y. P. Liu, M. Tang, L. Ma, R. X. Wang, L. Duan, *et al*., "Few-mode multicore fiber enabled integrated Mach-Zehnder interferometers for temperature and strain discrimination," *Optics Express*, 2018, 26(12): 15332–15342.

[18] C. X. Lu, J. Su, X. P. Dong, L. H. Lu, T. Sun, and K. T. V. Grattan, "Studies on temperature and strain sensitivities of a few-mode critical wavelength fiber optic sensor," *Journal of Lightwave Technology*, 2018, 19(5): 1794–1801.

[19] T. Huang, X. Shao, Z. Wu, Y. Sun, J. Zhang, H. Q. Lam, *et al*., "A sensitivity enhanced temperature sensor based on highly Germania-doped few-mode fiber," *Optics Communications*, 2014, 324: 53–57.

[20] L. V. Nguyen, D. Hwang, S. Moon, D. S. Moon, and Y. Chung, "High temperature fiber sensor with high sensitivity based on core diameter mismatch," *Optics Express*, 2008, 16(15): 11369–11375.

[21] B. Dong, D. Zhou, L. Wei, W. Liu, and J. Li, "Temperature- and phase-independent lateral force sensor based on a core-offset multi-mode fiber interferometer," *Optics Express*, 2008, 16(23): 19291–19296.

[22] D. Grobnic, C. W. Smelser, S. J. Mihailov, and R. B. Walker, "Long-term thermal stability tests at 1 000°C of silica fibre Bragg grating made with ultrafast laser radiation," *Measurement Science and Technology*, 2006, 17(5): 1009–1013.